John von Neumann Institute for Computing

Many-Body Coulomb Effects in the Optical Properties of Semiconductor Heterostructures

Torsten Meier, Bernhard Pasenow, Peter Thomas,
Stephan W. Koch

published in

NIC Symposium 2004, Proceedings,
Dietrich Wolf, Gernot Münster, Manfred Kremer (Editors),
John von Neumann Institute for Computing, Jülich,
NIC Series, Vol. **20**, ISBN 3-00-012372-5, pp. 261-270, 2003.

http://www.fz-juelich.de/nic-series/volume20

Many-Body Coulomb Effects in the Optical Properties of Semiconductor Heterostructures

Torsten Meier, Bernhard Pasenow, Peter Thomas, and Stephan W. Koch

Department of Physics and Material Sciences Center, Philipps University
Renthof 5, 35032 Marburg, Germany
E-mail: {Torsten.Meier, Bernhard.Pasenow, Peter.Thomas}@physik.uni-marburg.de
Stephan.W.Koch@physik.uni-marburg.de

The optical response of semiconductors is strongly influenced by the Coulomb interaction among the photoexcited carriers. Already in the linear optical regime the attraction between the oppositely charged electrons and holes introduces excitonic effects. A number of important many-body effects arising in linear and nonlinear optical spectroscopy can be described by microscopic theory within the framework of the semiconductor Bloch equations. Here, two examples which highlight Coulombic effects in semiconductor optics are briefly reviewed. First, signatures of four-particle biexciton correlations are investigated using coherent-excitation spectroscopy and it is shown how these signals are influenced by disorder. As a second example, excitonic effects in the absorption spectra of hybrid systems consisting of a photonic crystal and a semiconductor heterostructure are analyzed. It is shown, that the spatial periodicity of the photonic crystal leads to spatially periodic modulations of the optical and electronic properties of the semiconductor heterostructure. Many of the numerical results have been obtained using massively parallel computer programs which were run on the Cray T3E system in Jülich.

1 Introduction

To properly describe the optical properties of semiconductors one has to treat the dynamics of the light field, the material excitations, and their interactions. Since it is known from classical electrodynamics that the electric field couples to the polarization of a medium, the theoretical analysis of the material has to include this polarization as a key quantity[1].

Many aspects of the optical response of semiconductors can be described successfully by microscopic many-body theory[1]. Already in the linear optical regime the Coulomb interaction leads to characteristic signatures, i.e., the so called excitonic effects which are a consequence of the Coulomb attraction between photoexcited electrons and holes. To compute the nonlinear optical response, one has to treat a many-body problem introduced by the Coulomb interaction among the optically excited carriers. Although usually no fully exact treatment of the material response is possible, a number of approximation schemes have been developed and applied successfully to different excitation regimes, see, e.g., Refs. 1 and 2.

In the following, two examples which demonstrate the importance of Coulombic effects in semiconductor optics are briefly reviewed. In Sect. 2.1, signatures of four-particle biexciton correlations are investigated using coherent-excitation spectroscopy. It is analyzed how these signatures are influenced by disorder. As a second example, in Sect. 2.2 excitonic effects in the absorption spectra of hybrid systems which consist of a photonic crystal in the vicinity of a semiconductor heterostructure are analyzed. It is shown, that for such structures the spatial periodicity of the photonic crystal leads to spatially periodic modulations of the optical and electronic properties of the semiconductor heterostructure.

2 Examples

2.1 Biexciton Correlations in Semiconductor Heterostructures Viewed by Coherent-Excitation Spectroscopy

To study the coherent temporal dynamics of photoexcited systems one often uses four-wave mixing. Such an experiment can be performed using two short temporally-delayed laser pulses $\mathbf{E}_1$ and $\mathbf{E}_2$ which excite the sample from direction $\mathbf{k}_1$ at $t = 0$ and from direction $\mathbf{k}_2$ at $t = \tau$, respectively. Due to optical nonlinearities this excitation sequence results in a field that is diffracted in the direction $2\mathbf{k}_2 - \mathbf{k}_1$. For optically thin samples the measured time-resolved field intensity is proportional to $|P_{\mathrm{FWM}}(t,\tau)|^2$, where P_{FWM} is the polarization of the medium associated with the four-wave-mixing direction $2\mathbf{k}_2 - \mathbf{k}_1$, see Ref. 1.

Due to the loss of coherence (dephasing) the photoexcited polarization of the medium decays as function of time on a certain time scale. Hence, after the excitation with the two pulses also $P_{\mathrm{FWM}}(t,\tau)$ decays as function of t. For the case of semiconductor quantum wells with not too high light intensities, typical decays times are on the order of some ps, i.e., 10^{-12} s. If the pulses excite more than a single optical transition, $|P_{\mathrm{FWM}}(t,\tau)|^2$ shows modulations (beats) as function of t and in certain situations also as function of τ. Furthermore, in disordered system the four-wave-mixing signal is emitted as a photon echo, which means that the emitted field has a maximum at $t = 2\tau$, i.e., at the delay time after the second pulse. Studying the dynamics of $|P_{\mathrm{FWM}}(t,\tau)|^2$ as function of τ one gets information on the dynamical evolution of the polarization induced by the first pulse.

If both pulses have the same spectrum one calls the experiment degenerate. Coherent-excitation spectroscopy[3–6] is a particular example for a partially non-degenerate four-wave-mixing measurement. In this setup pulse, $\mathbf{E}_1$ is temporally long, i.e., spectrally narrow, whereas pulse $\mathbf{E}_2$ is short, i.e., spectrally broad. These experiments are called partially non-degenerate, since the spectra of the pulses are different but have a finite overlap. In coherent-excitation spectroscopy the long pulse $\mathbf{E}_1$ excites only transitions in a narrow spectral region around its center frequency ω_1. The short pulse $\mathbf{E}_2$ interacts with these transitions and produces further transitions within its broad spectral range. The four-wave-mixing signal is generated only by those transitions of the first and the second pulse which are optically coupled. Therefore, coherent-excitation spectroscopy is ideally suited to investigate coherent couplings among optical transitions.

To highlight the characteristic signatures of coherent-excitation-spectroscopy scans, Fig. 1 shows schematical results as they arise for the case of simple level systems. Displayed is the intensity of the Fourier-transform of the four-wave-mixing polarization $|P_{\mathrm{FWM}}(\omega,\omega_1)|^2$ which depends on the detection and the excitation frequency, ω and ω_1, respectively. For the case of a two-level system, Fig. 1(a), one sees a single peak in the coherent-excitation-spectroscopy scans. In this case, one only gets a strong signal if both the excitation and the detection energy coincide with the transition frequency of the two-level system. Due to homogeneous broadening which has been modeled by a dephasing time T_2, the line shape has a Lorentzian profile as function of both ω and ω_1, with a linewidth which is inversely proportional to T_2. For the case of two uncoupled two-level systems with different transition frequencies, the coherent-excitation-spectroscopy scans, Fig. 1(b), consist of two peaks which are both on the diagonal, i.e., at $\omega = \omega_1$. This is clear since each of the two uncoupled subsystems gives a single peak if both ω and ω_1 are equal

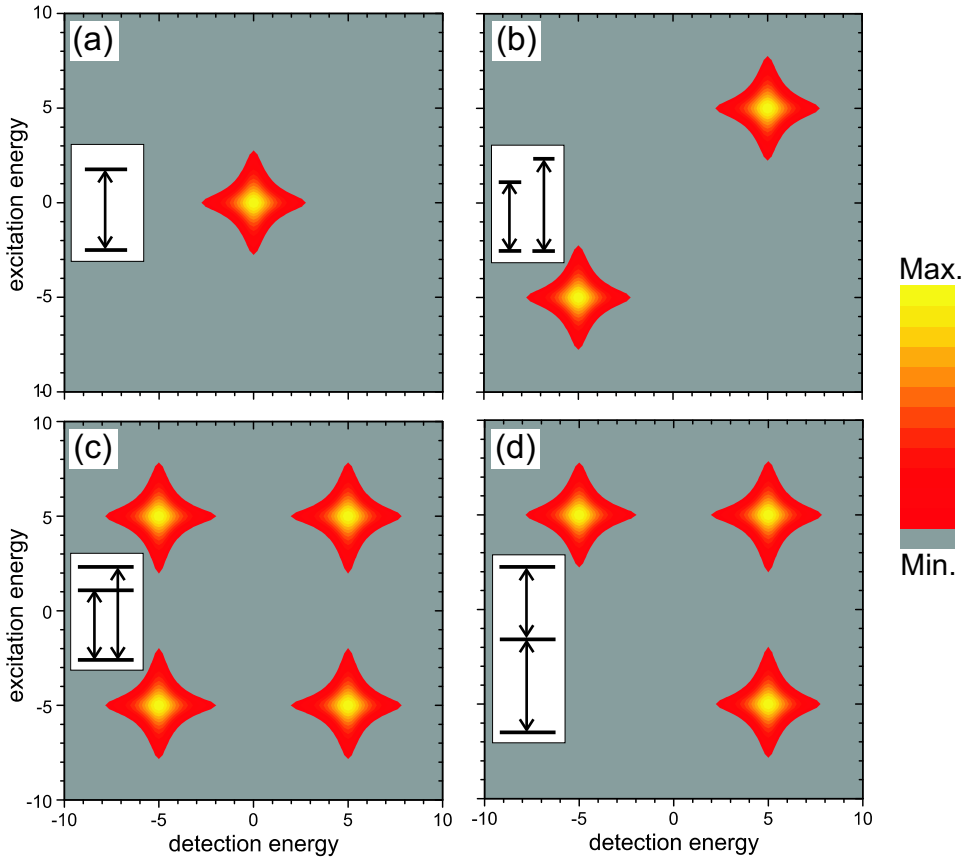

Figure 1. Schematical drawings of coherent-excitation-spectroscopy scans for homogeneously broadened level systems. Displayed is the Fourier-transform of the four-wave-mixing polarization $|P_{\mathrm{FWM}}(\omega,\omega_1)|^2$ as function of the detection and the excitation energies, $\hbar\omega$ and $\hbar\omega_1$, respectively. The color codes of the contour plot correspond to a logarithmic scale over 1.5 decades. (a) shows the result for a single two-level system, (b) for two-uncoupled two-level systems, and (c) for a three-level system, as indicated by the respective insets. (d) shows the result for a three-level system, where the energetically highest state is a two-photon resonance, see inset. Whereas the single-photon resonances represent transitions to excitons, the two-photon resonance is due to attractively interacting pairs of excitons, i.e., biexcitons.

to its transition frequency. If instead of two uncoupled two-level systems one investigates an intrinsically coupled system with two optical resonances, i.e., a three-level system, the coherent-excitation-spectroscopy scans change qualitatively. In this case ones does not only get two peaks on the diagonal, but additionally two peaks at off-diagonal positions, see Fig. 1(c). These two off-diagonal peaks occur if ω is equal to one transition frequency of the three-level system and ω_1 is equal to the other transition frequency. Therefore the four peaks in Fig. 1(c) are arranged at the corners of a square. Comparing Figs. 1(b) and 1(c) clearly shows that two systems which identical linear optical properties, which are characterized by two optical resonances, may have qualitatively different nonlinear optical properties. The appearance of the off-diagonal peaks Fig. 1(c) is due to the fact, that unlike

for two uncoupled two-level systems in the nonlinear dynamics of a three-level system the coherence between the two energetically highest states has to be considered.

Experimentally the situations considered in Figs. 1(a)-(c) have been investigated in semiconductor quantum well systems[3]. The two uncoupled resonances of Fig. 1(b) were realized using the exciton resonances of two spatially separated uncoupled quantum wells with different well width. As a realization of a three-level system, Fig. 1(c), the heavy- and light-hole exciton resonances of a single quantum well were used. Thus the results of Ref. 3 demonstrate that coherent-excitation spectroscopy can be used as an experimental tool to distinguish between coupled and uncoupled optical resonances.

As shown in Refs. 4–6, also biexcitons, i.e., bound states formed by the attractive interaction of two excitons, can be conveniently analyzed using coherent-excitation spectroscopy. For excitation configurations where transitions to biexcitons need to be considered, it was found that one gets a three peak signature in the coherent-excitation-spectroscopy scans. Two of these peaks appear if one resonantly excites the exciton resonance. In this case one get maxima at the positions of the exciton and the exciton to biexciton transition. Furthermore, a peak at the exciton frequency can also be induced by driving the system off-resonantly with a detuning below the exciton energy that matches the biexciton binding energy[4], i.e., the difference between the energy of the biexciton and twice the exciton energy, see Fig. 1(d) for a qualitative picture. Experiments and numerical calculations have shown that the heights of the two biexciton-induced peaks depend strongly on the polarization-directions of the incident pulses, on the dephasing times of the involved transitions, and, in particular, on the disorder present in the quantum wells[4,6].

In Ref. 6 coherent-excitation-spectroscopy scans were measured for quantum wells with different well widths using linear parallel polarization of the pulses. As usually, the disorder-induced inhomogeneous broadening originating from fluctuations of the well width is increasing with decreasing well width. On this set of samples it was thus possible to experimentally systematically analyze how the coherent-excitation-spectroscopy scans are influenced by disorder.

The measurements on the influence of disorder are qualitatively well reproduced by numerical results[6], that are obtained by solving microscopic equations of motion which include biexcitonic four-particle correlations in the coherent $\chi^{(3)}$-limit[2,5]. For homogeneously broadened transitions, i.e., vanishing disorder, one finds a strong response at the exciton for resonant excitation, see Fig. 2(a). The two biexciton-induced off-diagonal peaks, present in Fig. 1(d), do not appear as peaks in Fig. 2(a), but lead to the two shoulders extending from the exciton energy to lower excitation and detection energy, respectively. This is due to the fact that the biexciton-induced contributions are rather small for linear parallel polarization of the incident pulses. It is, however, possible to resolve the biexciton-induced peaks using linear perpendicular polarization of the incident pulses[4,5] . Note that for the case of homogeneously broadened transitions the spectral position of the maximum response is at the exciton energy and does not change significantly with excitation energy. For the case of rather big inhomogeneous broadening, the spectral position of the maximum response changes significantly with excitation energy and is always close to the diagonal, i.e., where excitation and detection energy are equal, see Fig. 2(c). In the intermediate case, where homogeneous and inhomogeneous broadening are comparable, one can even resolve two excitonic peaks in the spectra as function of detection energy when exciting above and below the exciton resonance, see Fig. 2(b). Since one of these two

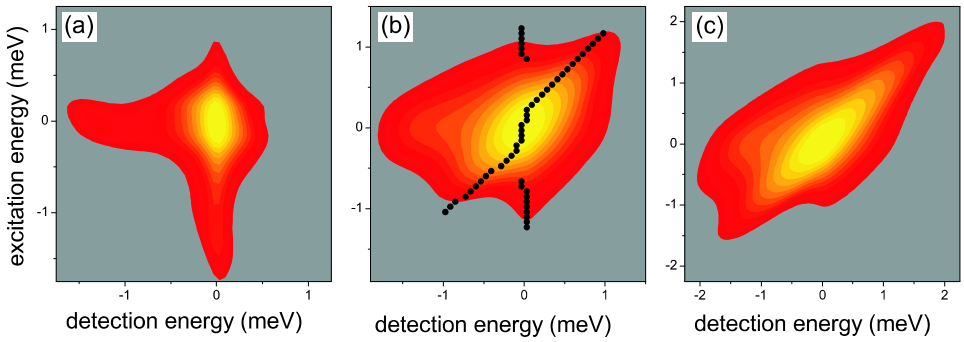

Figure 2. (a)-(c) Numerically calculated coherent-excitation-spectroscopy scans for linear parallel polarization of the incident pulses. The zero of the energy scale coincides with the exciton energy and the color codes extend over 2 decades on a logarithmic scale. The spectra are obtained solving microscopic equations of motion which include biexcitonic four-particle correlations in the coherent $\chi^{(3)}$-limit[2,5]. For (a) only homogeneous broadening has been considered. In (b) an asymmetric inhomogeneous broadening which decays exponentially with 0.3 meV and 0.4 meV below and above the exciton resonance, respectively, has been included. (c) same as (b) using doubled widths of 0.6 meV and 0.8 meV, respectively. The dots in (b) depict the signal maxima. After Ref. 6.

peaks is basically independent of excitation energy, whereas the other one is shifting with excitation energy and close to the diagonal, we hence find signatures arising from both the homogeneous and the inhomogeneous width in a single coherent-excitation-spectroscopy scan.

Further numerical investigations show that the appearance of the two excitonic peaks depends crucially on the spectra of the incident laser pulses and on the spectral shape and width of the inhomogeneous broadening. A detailed analysis of these effects could provide novel information on the influence of disorder on exciton spectra and optical nonlinearities in quantum wells.

2.2 Optical Properties of Semiconductor Photonic-Crystal Structures

Since the proposals by E. Yablonovitch[7] and S. John[8] in 1987, photonic crystals, i.e., spatially periodic arrangements of dielectrica, are the focus of intense worldwide research. One reason for this is that the periodic structuring of dielectric materials on the scale of the wavelength of light causes novel properties of the transverse part of electromagnetic fields. These include photonic band structures which have gaps for suitable geometries and strongly modify the photonic density of states.

Both, for fundamental research as well as for applications, it is very interesting to combine photonic crystals with the elementary optical excitations of atoms, molecules, and solids. Since the photoexcitations of matter are induced by the transverse part of the electromagnetic field, altering the properties of the electromagnetic field leads to a modified light-matter interaction, like, e.g., the suppression of spontaneous emission in a photonic band gap[9].

In this context, semiconductor heterostructures are very promising material systems, because they can be manufactured with almost atomic precision and they provide strong optical resonances due to excitons. These excitons are formed by the attractive interaction

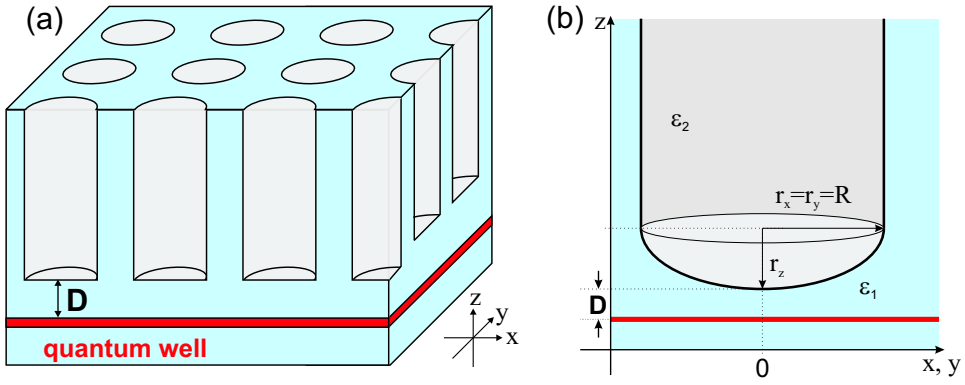

Figure 3. (a) Schematical drawing of the considered structure. A thin semiconductor quantum well (red) is embedded into dielectric material (light blue) and is separated the distance D from a two-dimensional photonic crystal, which is made of a periodic arrangement of air cylinders surrounded by a dielectric medium. (b) Detail of the model showing one cylinder with its elliptically shaped bottom. After Ref. 12.

between charged particles, i.e., electrons and holes, which is mediated by the longitudinal part of the electromagnetic field. Therefore, for a correct description of the optical resonances in a semiconductor heterostructure, it is important to adequately describe the longitudinal part of the electromagnetic field[10–13].

The model we chose for our analysis consists of a thin quantum well made of GaAs which is separated by a cap layer of thickness D from a two-dimensional photonic crystal made of air cylinders with radius R in a dielectric material. For a sketch of the system see Fig. 3(a). Since two-dimensional photonic crystals of this kind are manufactured by etching techniques, the bottom of the cylinder in not completely flat. Therefore, we describe it to have an ellipsoidal shape, where the longer axes r_x and r_y are matched to the cylinder radius R, see Fig. 3(b).

Due to image-charge effects, the energy of a charged particle in an environment of a spatially varying dielectric constant $\epsilon(\mathbf{r})$ becomes space dependent[10,11]. For our model, the periodicity of the photonic crystal introduces a periodic variation of the Coulomb self-energy $\delta V_0(\mathbf{r})$ in the semiconductor quantum well. As is shown in Fig. 4(a), $\delta V_0(\mathbf{r})$ is positive and has its biggest value at positions directly underneath the center of the cylinders, since here the distance to the quantum well is the smallest. Moving towards the perimeter of the cylinders $\delta V_0(\mathbf{r})$ decreases due to the increasing distance between the quantum well and the air.

Furthermore, the spatially varying dielectric constant $\epsilon(\mathbf{r})$ also influences the interaction between two charged particles[10,11]. As shown in Ref. 10, in a spatially inhomogeneous dielectric environment the generalized Coulomb potential $V_C(\mathbf{r},\mathbf{r}')$ depends explicitely on the two space coordinates $\mathbf{r}$ and $\mathbf{r}'$ and not just their distance. V_C can be written as $V_C(\mathbf{r},\mathbf{r}') = V(\mathbf{r},\mathbf{r}') + \delta V(\mathbf{r},\mathbf{r}')$, where $V(\mathbf{r},\mathbf{r}') = e\,e'/(\epsilon(\mathbf{r}')|\mathbf{r}-\mathbf{r}'|)$ is the usual statically screened interaction between two charges e and e' and the additional term $\delta V(\mathbf{r},\mathbf{r}')$ originates from induced surface polarizations at the interfaces which separate the regions of different ϵ. The periodicity of the photonic crystal introduces for the additive contribution δV of the generalized Coulomb potential a periodic variation with the center-of-mass

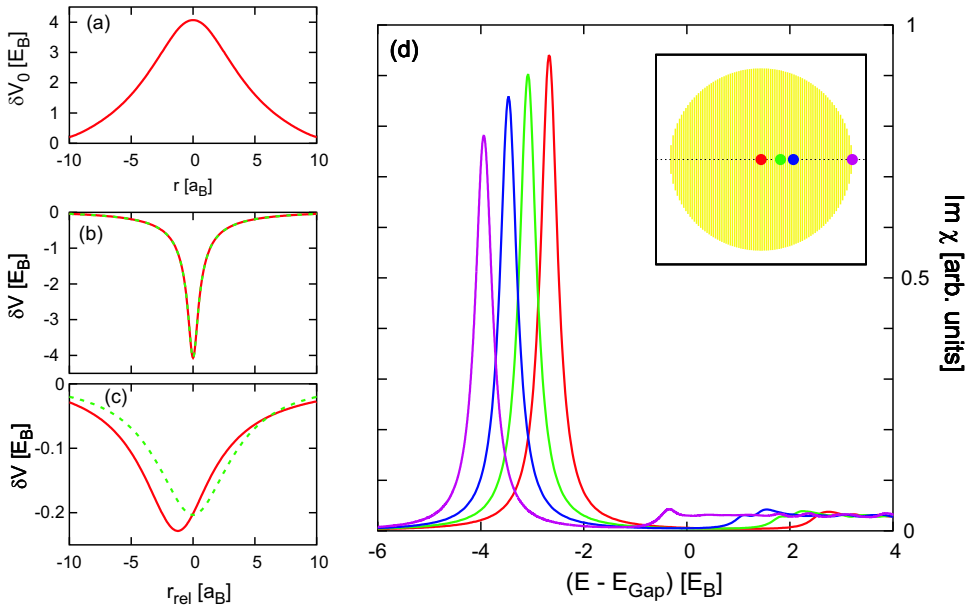

Figure 4. (a) Spatial variation of the Coulomb self-energy $\delta V_0(\mathbf{r})$ in the semiconductor quantum well as function of $\mathbf{r}_x$. E_B is the binding energy of a three-dimensional exciton and a_B its Bohr radius. The cap layer thickness is $D = 0.2\,a_B$, the radius of the air cylinders is $R = 10\,a_B$, the curvature of the bottom of the cylinders is characterized by $r_z = R/5$, and the surrounding dielectric medium is modeled using $\epsilon = 13.1$. (b) and (c) show calculated variations of the Coulomb interaction potential $\delta V(\mathbf{r}_{\rm COM}, \mathbf{r}_{\rm rel})$ induced by the photonic crystal for fixed center-of-mass positions. (b) shows δV for $\mathbf{r}_{\rm COM} = 0$, i.e., underneath the center of an air cylinder, and (c) is for $1.0\,R\,\mathbf{e}_x$, i.e., underneath the perimeter of an air cylinder. The solid red lines show the dependence of δV on the x-component of the relative coordinate for vanishing y-component, whereas the dashed green lines show the same for reversed x and y. (d) Calculated excitonic linear absorption spectra for the center-of-mass positions $\mathbf{r}_{\rm COM} = 0$ (red), $0.21\,R\,\mathbf{e}_x$ (green), $0.35\,R\,\mathbf{e}_x$ (blue), and $1.0\,R\,\mathbf{e}_x$ (magenta). The width of the resonances is due a phenomenological dephasing time. After Ref. 11.

coordinate $\mathbf{r}_{\rm COM}$. This spatial variation as function of the relative distance is illustrated in Fig. 4(b) and (c) for two different values of the center-of-mass coordinate. Clearly, δV is negative and has its largest values directly underneath the cylinders where the distance to the air is lowest and decreases when moving away from this position. In Fig. 4(c) one can see differences between the solid and dashed lines showing the anisotropy of the Coulomb potential resulting from the dielectric structuring.

The dependence of V_C on the center-of-mass position leads to local changes of the excitonic absorption spectra[10–13]. Examples of the calculated spatially-resolved excitonic absorption spectra are displayed in Fig. 4(d). Underneath the dielectric medium or directly below the boundary between the dielectric and air, the excitonic spectra are essentially identical to the homogeneous case without photonic crystal. Here, the two-dimensional quantum well exciton has a binding energy of $4\,E_B$ and the continuum absorption starts at the band gap energy $E = E_{\rm gap}$, see magenta line in Fig. 4(d). If one moves with the excitation towards positions underneath the air cylinders, as a results of the increasing self energy δV_0, see Fig. 4(a), the onset of the band gap moves towards higher energies.

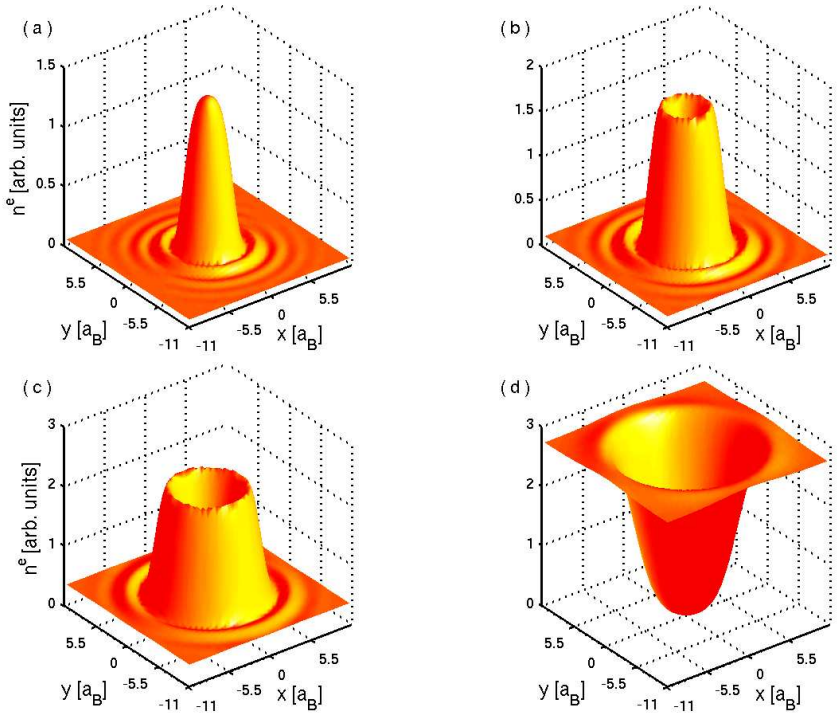

Figure 5. Normalized space-dependent electron populations in a quantum well excited resonantly using with a long, i.e., spectrally-narrow, and spatially-homogeneous laser pulse. The displayed populations are present at a time that is slightly before the incident pulse reaches its maximum. (a) exciting the highest energy exciton at $E = E_{\rm gap} - 2.6\,E_B$, (b) exciting at $E = E_{\rm gap} - 3.0\,E_B$, (c) exciting at $E = E_{\rm gap} - 3.4\,E_B$, and (d) exciting the lowest energy exciton at $E = E_{\rm gap} - 4.0\,E_B$.

For excitation directly underneath the center of an air cylinder, red line in Fig. 4(d), the continuum absorption is blue shifted to $E \approx E_{\rm gap} + 3\,E_B$ and also the exciton resonance appears at higher energies, $E \approx E_{\rm gap} - 2.7\,E_B$. However, the exciton binding energy, i.e., the energetic distance between the exciton to the onset of the continuum absorption, is increased to about $5.7\,E_B$. This is the result of the stronger attraction between electron and hole as described by δV, see Fig. 4(b). This increase in binding energy is also responsible for the higher absorption strength of the exciton in this case. Since the increase of the band gap is stronger than the increase in exciton binding energy, the spectral position of the exciton resonance shifts towards higher energies when moving the excitation towards positions underneath the air cylinders.

It has been shown that the spatially varying dielectric environment modifies the local excitonic absorption of a quantum well. This effect can be used to excite spatially inhomogeneous distributions of electrons and holes using a long, i.e., spectrally narrow, but spatially-homogeneous excitation pulses[12,13]. Calculated coherently-excited spatially-resolved electron populations are shown in Fig. 5. The computed populations depend strongly on the frequency of the spatially-homogeneous excitation pulse. If one excites

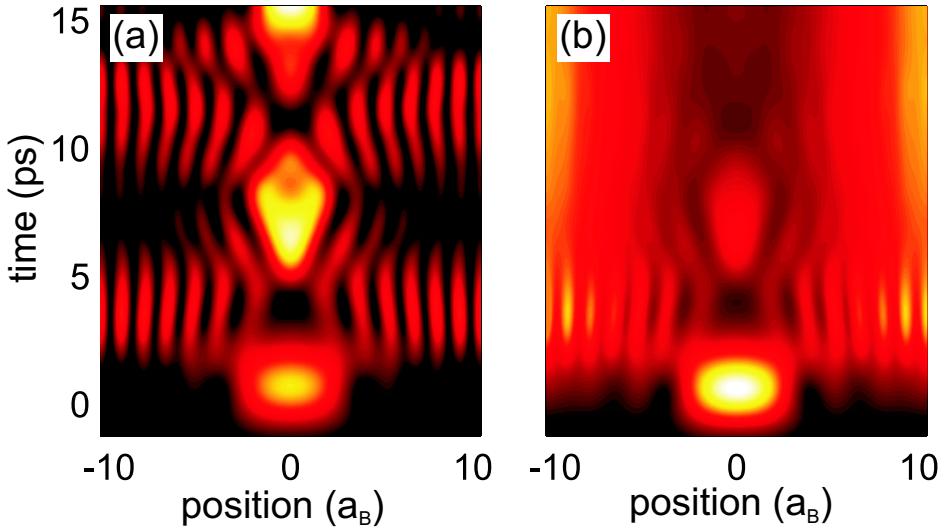

Figure 6. Contour plots showing the temporal evolution of the electron population in a one-dimensional quantum wire after coherent excitation with a long pulse with a central frequency tuned close to the highest exciton resonance. In (a) dephasing and thermalization has been neglected, i.e., the dynamics if fully coherent. In (b) dephasing and thermalization was phenomenologically modeled using time constants of $T_2 = 8\,\mathrm{ps}$ and $T_1 = 8\,\mathrm{ps}$ using a temperature of $T = 50\,\mathrm{K}$.

the energetically lowest exciton at $E = E_{\mathrm{gap}} - 4\,E_B$, see Fig. 5(d), the population is concentrated in the area outside the air cylinder, which is centered at $(0, 0)$. However, if the pulse excites the highest exciton resonance, $E = E_{\mathrm{gap}} - 2.6\,E_B$, the induced population is concentrated directly underneath the cylinder, see Fig. 5(a). In between these two extreme cases, e.g., for $E = E_{\mathrm{gap}} - 3.0\,E_B$ and $E = E_{\mathrm{gap}} - 3.4\,E_B$, we obtain a ring-like shape for the optically generated electron population, as shown in Figs. 5(b) and (c), respectively. These results demonstrate that it is indeed possible to use the spatial inhomogeneity induced by the dielectrically structured environment to optically create spatially inhomogeneous, periodically varying carrier populations.

Now we investigate the temporal evolution of the electron populations after exciting close to the highest exciton resonance. To keep the numerical complexity within reasonable limit, we have used a one-dimensional quantum wire instead of the quantum well. In Fig. 6(a), at $t \approx 0$ the electrons are created directly underneath the center of the air cylinders. Due to coherent wave packet dynamics, they move with increasing time first outwards, i.e., to regions in between the cylinders, then in the opposite direction, and after about 7 ps they accumulate at the position where they were optically created and this cycle starts over again. The transient transition from the coherent to the incoherent regime is investigated using time constants T_2 and T_1 which model the decay (dephasing) of the polarization and the thermalization of the population, respectively. Including dephasing and thermalization, changes the dynamics of the electron population significantly, see Fig. 6(b). On the one hand, the coherent wave packet oscillations are suppressed with increasing time. On the other hand, in the long time limit the electrons accumulate at the positions where the self energy δV_0 is lowest, i.e., in between the cylinders.

3 Summary

Two examples are presented which show that Coulombic many-body effects have a strong influence on semiconductor optics. Many of our recent numerical results on the examples discussed here and on other topics were obtained using massively parallel computer programs which were run on the Cray T3E system in Jülich. Presently, our grant on this machine allows us to use 3027 hours of computer time per month. Furthermore, we recently started to use the new IBM-Regatta JUMP system for which we have a quota of 1500 hours of computer time per month.

Acknowledgments

This work is supported by the Deutsche Forschungsgemeinschaft through the Schwerpunktsprogramm "Photonische Kristalle", by the Max Planck Research prize of the Humboldt and Max Planck societies, and by the Center for Optodynamics, Philipps-University Marburg. We thank the John von Neumann-Institut für Computing (NIC), Forschungszentrum Jülich, Germany, for grants of computer time on their supercomputer systems.

References

1. H. Haug and S.W. Koch, "Quantum Theory of the Optical and Electronic Properties of Semiconductors", 3rd ed., World Scientific Publ., Singapore (1994).
2. T. Meier and S.W. Koch, in Semiconductors and Semimetals, Vol. **67**, "Ultrafast Physical Processes in Semiconductors", pp. 231-313, Academic Press (2001).
3. A. Euteneuer, E. Finger, M. Hofmann, W. Stolz, T. Meier, P. Thomas, S.W. Koch, W.W. Rühle, R. Hey, and K. Ploog, Phys. Rev. Lett. **83**, 2073 (1999).
4. E. Finger, S.P. Kraft, M. Hofmann, T. Meier, S.W. Koch, W. Stolz, and W.W. Rühle, phys. stat. sol. (b) **234**, 424 (2002).
5. T. Meier, C. Sieh, S. Weiser, M. Reichelt, C. Schlichenmaier, S. Siggelkow, P. Thomas, and S.W. Koch, John von Neumann Institute for Computing, Jülich, Germany, NIC Series Vol. **9**, 315 (2002).
6. T. Meier, C. Sieh, E. Finger, W. Stolz, W.W. Rühle, P. Thomas, and S.W. Koch, phys. stat. sol. (b) **238**, 537 (2003).
7. E. Yablonovitch, Phys. Rev. Lett. **58**, 2059 (1987).
8. S. John, Phys. Rev. Lett. **58**, 2486 (1987).
9. M. Kira, W. Hoyer, T. Stroucken, and S. W. Koch, Phys. Rev. Lett. **87**, 176401 (2001).
10. T. Stroucken, R. Eichmann, L. Banyai, and S. W. Koch, Journ. Opt. Soc. Am. B **19**, 2292 (2002).
11. R. Eichmann, B. Pasenow, T. Meier, T. Stroucken, P. Thomas, and S. W. Koch, Appl. Phys. Lett. **82**, 355 (2003).
12. R. Eichmann, B. Pasenow, T. Meier, P. Thomas, and S. W. Koch, phys. stat. sol. (b) **238**, 439 (2003).
13. T. Meier and S.W. Koch, in "Photonic Crystals: Advances in Design, Fabrication and Characterization", Eds. K. Busch, S. Lölkes, R.B. Wehrspohn, and H. Föll, Wiley (2004), to be published.